# FIRST EDGE-LOCALIZED MODE SUPPRESSION WITH LOWER HYBRID WAVES ON THE EAST TOKAMAK

Shaocheng Liu<sup>1,2</sup>, Yunfeng Liang<sup>3,4\*</sup>, Rui Ding<sup>3\*</sup>, Manni Jia<sup>3</sup>, Fuqiong Wang<sup>1,2</sup>, Ning Yan<sup>3</sup>, Miaohui Li<sup>3</sup>, Yifeng Wang<sup>3</sup>, Xiaohe Wu<sup>3</sup>, Li Li<sup>1,2</sup>, Mengze Xu<sup>1,2</sup>, Tonghui Shi<sup>3</sup>, Liang Liao<sup>3</sup>, Wenyin Wei<sup>3,4</sup>, Genfan Ding<sup>3</sup>, Shuai Xu<sup>4</sup>, Long Zhang<sup>1,2</sup>, Yifei Jin<sup>3</sup>, Qing Zang<sup>3</sup>, Lingyi Meng<sup>3</sup>, Gongshun Li<sup>3</sup>, Tao Zhang<sup>3</sup>, Ziqiang Zhou<sup>3</sup>, Ran Chen<sup>3</sup>, Hailin Zhao<sup>3</sup>, Youwen Sun<sup>3</sup>, Long Zeng<sup>5</sup>, Huiqian Wang<sup>6</sup>, Tengfei Tang<sup>6</sup>, Rong Yan<sup>3</sup>, Liang Wang<sup>3</sup>, Guoqiang Li<sup>3</sup>, Guosheng Xu<sup>3</sup>, Jinping Qian<sup>3</sup>, Xianzu Gong<sup>3</sup>, Xiang Gao<sup>3</sup>, Fangchuan Zhong<sup>1,2</sup> and EAST Team

- <sup>1</sup>College of Physics, Donghua University, Shanghai, China.
- <sup>2</sup>Member of Magnetic Confinement Fusion Research Centre, Ministry of Education, China.
- <sup>3</sup> Institute of Plasma Physics, Chinese Academy of Sciences, Hefei, China.
- <sup>4</sup> Forschungszentrum Jülich GmbH, Jülich, Germany.
- <sup>5</sup> Department of Engineering Physics, Tsinghua University, Beijing, China.
- <sup>6</sup> General Atomics, San Diego, California, United States of America

Email: y.liang@fz-juelich.de, rding@ipp.ac.cn

#### **Abstract**

We report the first successful suppression of edge-localized modes (ELMs) achieved through lower hybrid wave (LHW) on the EAST tokamak. The spatial structure of the helical current filaments (HCFs) induced by LHW is directly measured using a directional electron probe, and a plasma density threshold for driving HCFs is observed. An accurate 3D HCFs model is constructed based on these measurements, and the simulation results are consistent with the radial magnetic field perturbation and the divertor heat flux footprint in experiment. The experimental scenario is optimized according to the experimental results and the HCFs model, and ELM suppression is achieved by LHW modulation on EAST. The RMP spectrum of HCFs has good resonant features and the predominant perturbation mode is n = 1, with a normalized radial field perturbation in the order of  $10^{-3}$ . Edge turbulence and cross-field transport are significantly enhanced when the ELM is suppressed.

## 1. INTRODUCTION

Edge-localized mode (ELM) [1, 2], an intense and periodic magnetohydrodynamic (MHD) instability in the edge region of H-mode, is characterized by the collapse of edge transport barrier, large amounts of heat and particle exhaust, and high transient heat load on the first wall, which is a critical challenge for the safety and lifetime of materials in large-scale tokamaks, such as ITER and fusion reactors [3]. It is therefore a key issue to control ELM and avoid damage to materials in magnetically controlled fusion devices. Resonant magnetic perturbation (RMP), usually driven by external coils, is an effective technique to mitigate or suppress ELM by creating a stochastic edge region through the overlap of magnetic islands, which has been demonstrated in many tokamaks, such as DIII-D [4], JET [5], ASDEX-Upgrade [6, 7], MAST [8], KSTAR [9, 10], EAST [11] and HL-2A [12].

Lower hybrid waves (LHWs) are a demonstrated and continuous means of driving toroidal current via accelerating fast electrons in tokamaks [13-15]. In 2012, ELM mitigation was achieved by LHW modulation on EAST for the first time [16, 17], offering an alternative way to control ELM without undermining the useful feature of pedestal [18]. Similar to the external coils, LHWs drive helical filament currents (HCFs) in the SOL, generate RMPs in edge plasma and change magnetic topology, increase cross-field transport and avert the crash of large ELMs [16]. With these interpretations, a physical model is used to characterize the HCFs structure and edge magnetic topology changes, which is consistent with the experimental observations [19, 20]. LHWs could also increase edge turbulence and radial transport [21], and broaden the divertor heat flux width [22]. Since ELM mitigation or suppression requires a good RMP spectrum and sufficient amplitude, it is difficult to access

the plasma conditions for ELM suppression without accurate characterization of HCFs [23]. Consequently, to achieve reliable and stable control of the ELM with LHWs, we still need to know the spatial structure of the HCFs and their dependence on key plasma parameters.

In this paper, we measure the radial profiles of the HCFs of LHWs with a new diagnostic and reconstruct a fine HCFs model from experiment. Then, we develop the scenario of ELM control with LHW modulation, and achieve first stable ELM suppression in EAST tokamak. The RMP spectrum and edge turbulence evolution are presented to reveal the mechanism in the ELM control experiment.

## 2. MEASUREMENT AND MODELLING OF HCFs

A directional electron probe (DEP) has been developed to directly measure the SOL current driven by LHWs [24, 25]. As shown in Figure 1 (a) and (b), the DEP has 6 radial channels spaced by 5 mm, and each channel is equipped with two opposite collectors. The collector, embedded inside a pinhole with a width of 0.5 mm and a depth of 3 mm, is biased to 200 eV to repel low energy ions, and the high energy ions are blocked by the wall of the pinhole due to their large Larmor radii, therefore the collected current is mainly contributed by electrons. The net current carried by non-thermal electrons is obtained by taking the difference between two opposite collected currents. The principle of the DEP is validated by a particle trajectory simulation [24] and a commissioning experiment [25] on EAST.

To measure the radial profile of HCFs, the DEP is plunged into the edge plasma and stays at the innermost position for 500 ms. Simultaneously the 4.6 GHz LHW heating power is set to 1 MW and modulated with a 10 Hz frequency, 50% duty cycle and 90° phase difference of LHW waves [26]. The SOL current measured

by all DEP channels are presented in Figure 1 (c). In each LHW modulation cycle, it can be seen that the SOL current increases from a low value to a maximum of 20 A/cm<sup>2</sup> after the LHW is turned on, and the SOL current drops dramatically when the LHW is turned off. The radial profiles of the SOL current for three plasma-averaged density cases are given in Figure 1 (d). For the LHW-off phase, the SOL current increases with the lineaveraged density ( $n_e = 2-3.6 \times 10^{19} \text{ m}^{-3}$ ) from almost 0 to 5 A/cm<sup>2</sup>. In LHW-on phase, the maximum of SOL current is 1 A/cm² in the  $n_e = 2 \times 10^{19}$  m<sup>-3</sup> case, which has almost the same amplitude and radial profile as that in LHW-off case. However, the maxima of SOL current in  $n_e = 3$  and  $3.6 \times 10^{19}$  m<sup>-3</sup> cases increase significantly to 15 and 24 A/cm<sup>2</sup> when LHW is turned on. In high density cases, the HCFs driven by LHW cover a radial range of 25 mm and peak at R = 2335 mm (15 mm inward from the low-field side limiter) with an amplitude larger than 20 A/cm<sup>2</sup> in anti-clockwise direction viewed from top. More importantly, a plasma density threshold (around  $n_e = 3 \times 10^{19} \,\mathrm{m}^{-1}$ <sup>3</sup> for 4.6 GHz LHW on EAST) required to drive considerable LHW HCFs is discovered, which is a key dependence of HCFs on plasma parameters

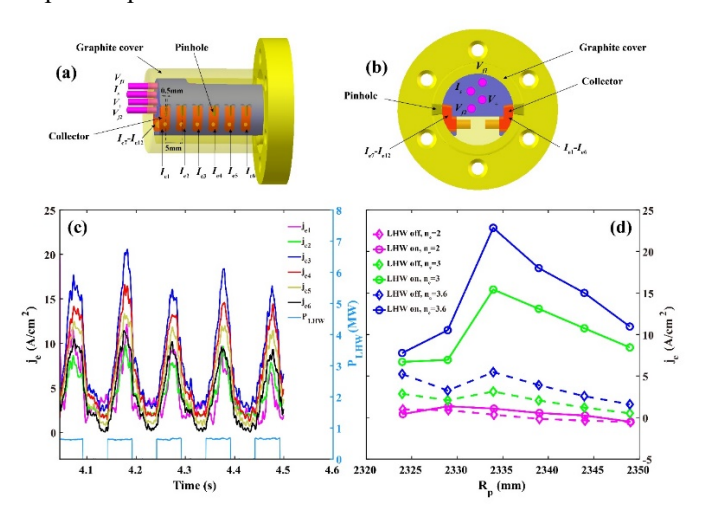


Figure 1. SOL current induced by LHW and the sketch of DEP. (a) Right view of DEP. (b) Front view of DEP. (c) Temporal evolution of the SOL current density measured by DEP, and the LHW heating power shown in light blue. (d) Radial profiles of the SOL current density induced by LHW for three plasma lineaveraged density cases.

According to the radial profile of the SOL current induced by LHWs in  $n_e = 3.6 \times 10^{19}$  m<sup>-3</sup>, the 3D structure of the HCFs is reconstructed. The 4.6 GHz LHW antenna of EAST consists of four arrays along the poloidal direction, as illustrated in Figure 2 (d). In consequence, we assume that the HCFs originate from the front of the LHW antenna, i.e., at the same poloidal angle as the antenna arrays. Since the electron density and temperature are almost constant on a flux surface, we also assume that the current density of the HCFs is the same on a flux surface. With these settings, the poloidal section in front of the LHW antenna is divided into 40 (poloidal) × 20 (radial) mesh grids, with the area S, current density j and current I = jS of the grids illustrated in Figure 2 (a-c), respectively. The total current of the HCFs is 3.16 kA, with a distance of 10-35 mm outside the LCFS. Starting from these grids, the 3D structure of HCFs is reconstructed by field line tracing [27], as shown in Figure 3. The HCFs induced by four antenna arrays are illustrated in different colors, and the yellow HCFs are measured by DEP. In this way, a fine physical model of the HCFs is built up from experiments. A series of simulation results are well consistent with the radial magnetic field perturbation and the divertor heat flux footprint in experiment, demonstrating the validity and accuracy of the HCFs model.

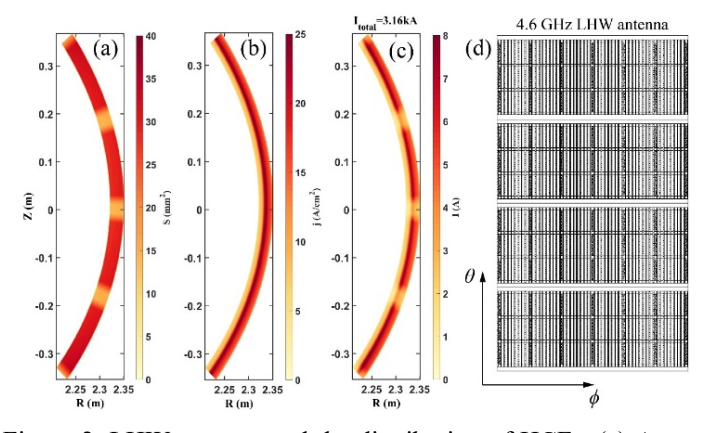


Figure 2. LHW antenna and the distribution of HCFs. (a) Area of mesh grids in front of the LHW antenna. (b) SOL current density of the grids. (c) SOL current of the grids. (d) Structure of the 4.6 GHz LHW antenna on EAST (viewed from the machine center).

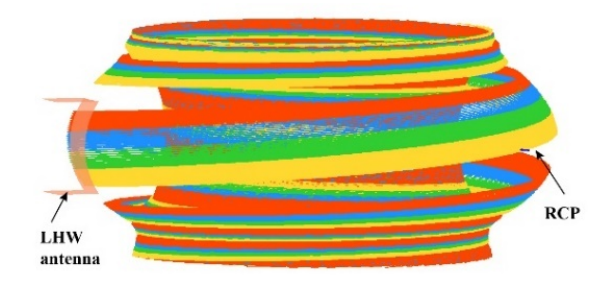


Figure 3. Three-dimensional structure of HCFs, with four arrays of LHW antenna illustrated in different colors. RCP denotes the position of the reciprocating probe.

## 3. ELM SUPPRESSION WITH LHWS

Experimental scenario of ELM control with LHW is optimized based on the HCFs model and its dependence on plasma density. A series of ELM control experiments by LHW modulation have been carried out on EAST with line-averaged density  $n_e = 3.5$ -5.5×10<sup>19</sup> m<sup>-3</sup>, safety factor at the 95% normalized poloidal flux surface  $q_{95} = 4.6-6.5$ , electron cyclotron resonance heating (ECRH) power 1.5-2 MW, neutral beam injection (NBI) heating power 1.5-2 MW, LHW heating power 1-1.5 MW and modulation frequency 5-10 Hz. ELM suppression is achieved for  $q_{95} = 5.6-6.2$  is presented in Figure 4. When LHW is turned on, the regular ELMs are suppressed after a short time. A typical discharge for the  $q_{95} = 4.6$  case is shown in Figure 5. In the LHW-off phase, regular ELMs are observed with a frequency around 100 Hz, causing high transient particle flux on divertor target. When the LHW is switched on, the plasma enters an ELM-free region after a short time (10-20 ms), clear density pump-out is observed, and the baselines of divertor particle flux and  $D_{\alpha}$  emission intensity increase sharply at the onset of ELM suppression, indicating the enhancement of cross-field transport and divertor particle deposition compared to the inter-ELM phase. The radial profiles of electron density and temperature are

fitted according to the Thomson scattering and reflectometry measurements [28, 29]. Compared with the LHW-off case, the ELM suppression phase with LHW has a lower electron density but almost the same electron temperature in the pedestal, consistent with the enhanced particle deposition in divertor. However, the electron temperature is higher at the pedestal top and in the core region for the LHW-on case, leading to a significant increase of electron pressure and plasma stored energy in the core plasma. The enhanced cross-field transport and the slight decrease of electron pressure in the pedestal contribute to the maintenance of ELM suppression.

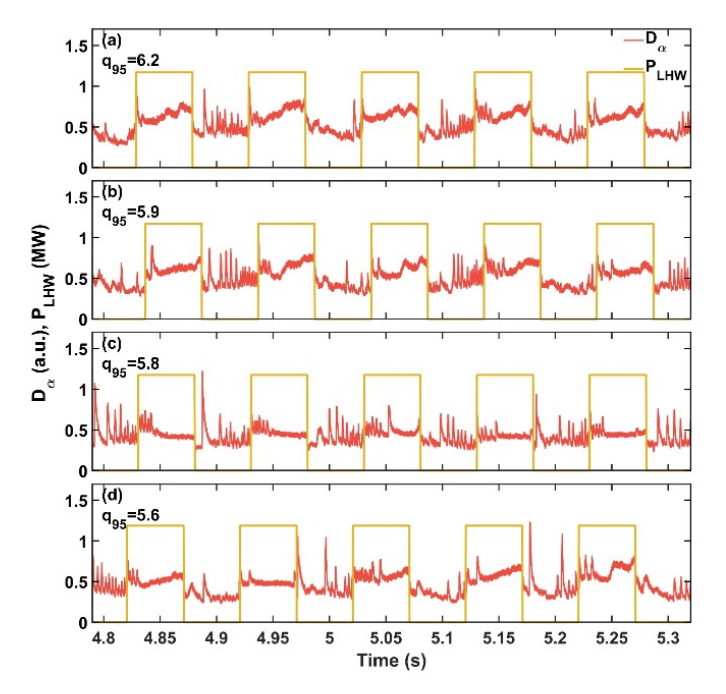


Figure 4. ELM suppression with LHWs modulation in window of  $q_{95} = 5.6$ -6.2. The red curves are  $D_{\alpha}$  emission intensity, and the yellow curves are LHW heating power.

HCFs model is also built from the SOL current profiles measured by DEP in ELM suppression. The spectrum of magnetic field perturbation from HCFs is calculated by the framework of MAPS. The distribution of normalized radial field perturbation  $B^{\rho}/B^{\zeta}$  in poloidal mode (m) and toroidal mode (n) space is illustrated in Figure 6 (a). The predominant toroidal mode number is n = 1 with  $(B^{\rho}/B^{\zeta})_{m=6,n=1} = 3.4 \times 10^{-4}$ , which is about 10 times larger than that of n = 3 and 5. The perturbation components of even toroidal mode numbers are 1-2 orders of magnitude smaller than those of odd toroidal mode numbers. The radial distributions of  $(B^{\rho}/B^{\zeta})_{mn}$  in n = 1, 2, 3, 5 are presented in Figure 6 (b-e), respectively. Radial profile of the largest normalized perturbation field follows the shape of the safety factor q in all the four cases, manifesting a very good resonant feature with the resonant surfaces at the plasma edge. In addition, the maximum of  $(B^{\rho}/B^{\zeta})_{mn}$  is shifted to high poloidal mode number m as the toroidal mode number n increases. Compared with the RMP spectrum driven by external coils on EAST [30, 31], the magnetic topology induced by LHW has a better resonant spectrum, because the HCFs follow the SOL field line and are closer to the edge plasma than the external coils.

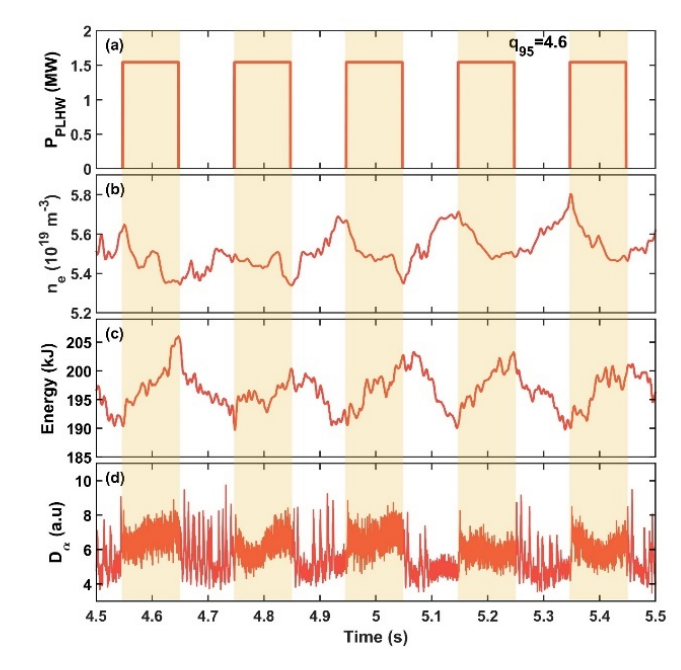


Figure 5. Plasma parameters of the ELM control experiment with LHW modulation for  $q_{95} = 4.6$  case. (a) LHW heating power, with the yellow shaded rectangle denoting the LHW on phase. (b) plasma averaged density. (c) plasma stored energy. (d)  $D_{\alpha}$  emission intensity.

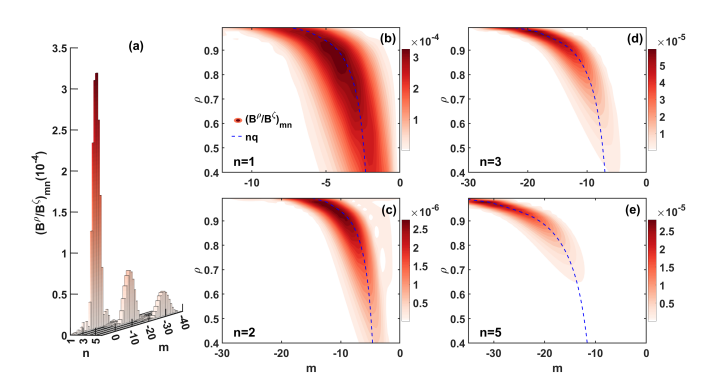


Figure 6. Spectra of normalized perturbation field driven by HCFs when ELM is suppressed. (a) Distribution of  $(B^{\rho}/B^{\zeta})_{mn}$  in m and n space. (b-e) Radial profiles of the spectrum of  $(B^{\rho}/B^{\zeta})_{mn}$  for n=1,2,3 and 5 components.  $\rho$  and  $\zeta$  are normalized radial coordinate and toroidal angle in PEST flux coordinate, respectively. The blue dashed line in (b-e) is the safety factor.

## 4. EDGE TURBULENCE AND TRANSPORT

Edge turbulence evolution in ELM control experiment is measured by gas puff imaging [32] and electron cyclotron emission (ECE) [33] diagnostics, as shown in Figure 7. When LHW is switched on at 5.26 s, ELMs and their bright vertical power spectra in the GPI and ECE signals disappear shortly, an edge coherent mode (ECM) around 17 kHz appears, and the broadband turbulence up to 100 kHz in the edge plasma is enhanced significantly. The ECM is distinct in the pedestal region, becomes weak at the LCFS, and almost disappears in the SOL. In addition, the ECM is absent in the ECE channels in the core plasma, indicating that this mode is located in the pedestal region. The toroidal mode number of the ECM derived from two

toroidal magnetic coil arrays is n = 1. The turbulence propagation velocity can be calculated by the time-delay estimation method (TDE) from GPI [34], as presented in Figure 7 (g) and (h) for the radial and poloidal velocities, respectively. In the ELMy phase without LHW, the turbulence radial velocity is small in the SOL, increases with the decreasing  $\rho$  inside the LCFS, and reaches a maximum at  $\rho = 0.95$ ; the turbulence poloidal velocity is small and toward the ion-diamagnetic drift direction in the near SOL, and increases gradually with the decreasing  $\rho$  along the electron-diamagnetic drift direction. Note that the decrease of turbulence velocity in the range of  $\rho$  < 0.94 is mainly due to the weak GPI emission intensity and the large uncertainty from TDE method in this region. In contrast, during ELM suppression with LHW, the turbulence radial velocity is higher in the SOL, and there is a notable trough at  $\rho = 0.96$ ; the positive  $V_{\theta}$  in the pedestal region is much higher than that of the LHW-off case. The radial electric field  $E_r = V_\theta B_\phi$  also has more negative value in the LHW-on case. To summarize, the edge plasma fluctuation level is much higher in the pedestal and the near SOL during ELM suppression, the turbulence poloidal and radial velocities are much higher around the LCFS, which could contribute to outward cross-field transport. In the previous work on EAST, broadband turbulence could drive significant radial heat and particle transport during ELM mitigation and suppression by RMP coils [35, 36], and the ECM provides continuous radial transport in H-mode plasma [37, 38]. In our experiment, the edge radial turbulent transport increased significantly when LHW is switched on, as shown in Figure 8.

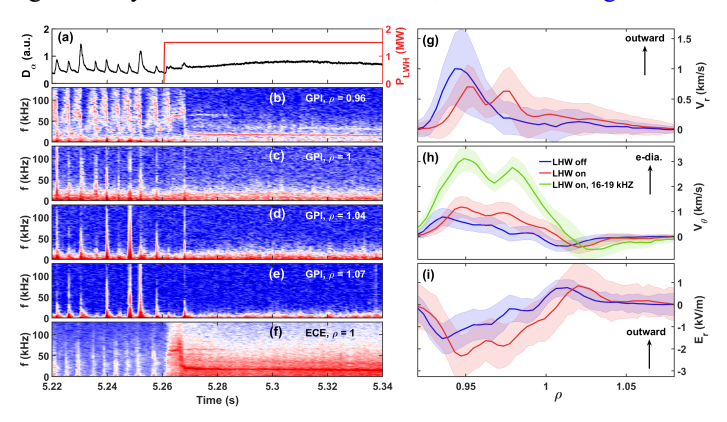


Figure 7. Frequency spectrogram of GPI and ECE signals in ELM control experiment. (a)  $D_{\alpha}$  emission intensity (black) and LHW heating power (red). (b-e) Auto-correlation power spectra of GPI fluctuations at  $\rho=0.96$ -1.07. (f) Auto-correlation power spectrum of ECE fluctuations at  $\rho=1$ . (g) Turbulence radial velocity, (h) turbulence poloidal velocity and (i) radial electric field derived from GPI fluctuations for LHW-off and LHW-on cases. The green curve in (h) is calculated from the GPI fluctuations in 16-19 kHz.

## 5. SUMMARY

We have successfully achieved stable ELM suppression by using LHW modulation with  $q_{95} = 4.6$ -6.5 on EAST tokamak. First, the spatial structure of HCFs induced by LHW is directly measured by a newly developed DEP diagnostic, covering a radial region of about 25 mm and a maximum current density above 20 A/cm². A density threshold is discovered to generate considerable LHW HCFs in our experiment, which is the key dependence of HCFs on plasma parameters. Based on these

experimental results, a fine 3D HCFs model is reconstructed by the field line tracing, and the magnetic topology induced by HCFs is analyzed by the MAPS code. With an optimized experimental scenario, stable ELM suppression is achieved in a series of experiments with line-averaged density  $n_e = 3.5$ -5.5×10<sup>19</sup> m<sup>-3</sup>, LHW heating power 1-1.5 MW and modulation frequency 5-10 kHz. The normalized radial magnetic field perturbation has very good resonant features with the resonant surfaces at the plasma edge, with a predominant perturbation mode n = 1 and an amplitude  $B^{\rho}/B^{\zeta}$  in the order of  $10^{-3}$  During ELM suppression, the pedestal density decreases significantly, leading to a slightly smaller electron pressure gradient, which moves the pedestal plasma from the stability boundary of the P-B mode to a stable region, i.e., from ELMy plasma to ELM-free plasma. In addition, the SOL electron density and temperature, as well as divertor particle deposition increase significantly in the ELM suppression phase compared to the ELMy phase, indicating enhanced cross-field transport in the edge plasma, which is crucial for maintaining the lower pedestal plasma density in the ELM-free phase. Edge broadband turbulence is enhanced greatly and an ECM is observed in the pedestal region during ELM suppression, which could drive outward cross-field transport. Since ITER has a much higher plasma density in the core and edge plasma than EAST, the SOL current driven by LHCD could be much larger, therefore it is possible to control ELMs and its high transient divertor heat load by using LHWs in the steady-state operation of ITER.

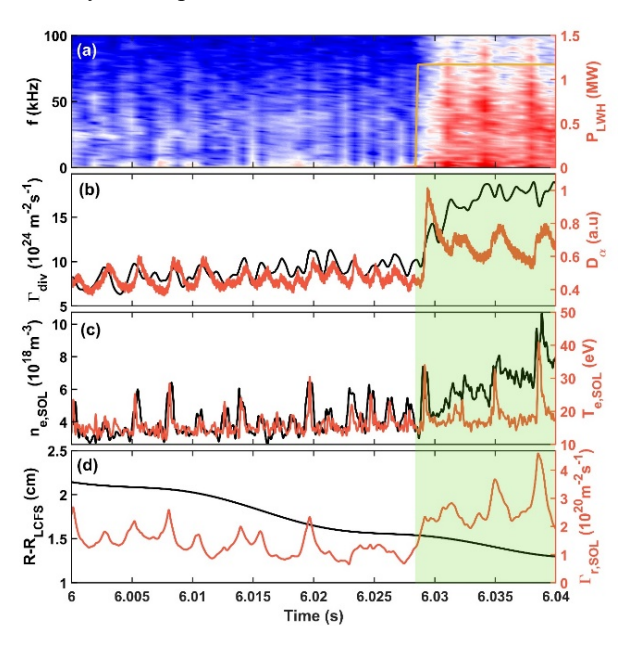


Figure 8. Temporal evolution of edge parameters during LHW modulation. (a) Auto-correlation power spectra of edge ECE signal. (b) Divertor particle flux and  $D_{\alpha}$  signal. (c) SOL electron density and temperature measured by reciprocating probe. (d) Radial position of probe and radial turbulent particle flux.

# Acknowledgements

The authors would like to acknowledge the support and assistance from the EAST team. This work was supported by the National Key R&D Program of China under grant No. 2024YFE03010000, the National Natural Science Foundation of China under grant No. 12275310, the Open Fund of Magnetic Confinement Fusion Laboratory of Anhui Province under grant

No. 2024AMF04001 and the Central Universities under grant No. 232024G-10.

#### Reference

- [1] Wagner F. et al 1982 Phys. Rev. Lett. 49 1408
- [2] Zohm H. 1996 Plasma Phys. Control. Fusion. 38 105
- [3] Bigot B. 2019 Nucl. Fusion 59 112001
- [4] Evans T. E. et al 2004 Phys. Rev. Lett. 92 235003
- [5] Liang Y. et al 2007 Phys. Rev. Lett. 98 265004
- [6] Suttrop W. et al 2011 Phys. Rev. Lett. 106 225004
- [7] Willensdorfer M. et al 2024 Nat Phys 20 s41567
- [8] Kirk A. et al 2011 Plasma Phys. Control. Fusion. 53 065011
- [9] Jeon Y. M. et al 2012 Phys. Rev. Lett. 109 035004
- [10] Kim S. K. et al 2024 Nat Commun 15 3990
- [11] Sun Y. et al 2016 Phys. Rev. Lett. 117 115001
- [12] Sun T. F. et al 2021 Nucl. Fusion 61 036020
- [13] Fisch N. J. 1978 Phys. Rev. Lett. 41 873
- [14] Fisch N. J. et al 1992 Phys. Rev. Lett. 69 612
- [15] Fisch N. J. 1987 Rev Mod Phys 59 175
- [16] Liang Y. et al 2013 Phys. Rev. Lett. 110 235002
- [17] Li J. et al 2013 Nat Phys 9 817
- [18] Morris W. 2013 Nat Phys advance online publication nphys2825
- [19] Xu S. et al 2018 Nucl. Fusion 58 106008
- [20] Rack M. et al 2014 Nucl. Fusion 54 064016
- [21] Chen R. et al 2015 Nucl. Fusion 55 033012
- [22] Deng G. Z. et al 2021 Nucl. Fusion 61 106015
- [23] Yang Q. Q. et al 2019 Plasma Phys. Control. Fusion. 61 065023
- [24] Liu S. C. et al 2021 Nucl. Fusion 61 126004
- [25] Liu S. C. et al 2021 Nuclear Materials and Energy 29 101080
- [26] Li M. H. et al 2020 23rd Topical Conference on Radiofrequency Power in Plasmas 2254 080005
- [27] Jia M. et al 2018 Nucl. Fusion 58 046015
- [28] Zang Q. et al 2010 Plasma Sci. Technol. 12 144
- [29] Wang Y. M. et al 2019 Fusion Eng. Des. 148 111286
- [30] Sun Y. et al 2017 Nucl. Fusion 57 036007
- [31] Sun Y. et al 2021 Nucl. Fusion 61 106037
- [32] Liu S. C. et al 2022 Fusion Eng. Des. 179 113156
- [33] Zhao H. L. et al 2018 Rev. Sci. Instrum. 89 10h111
- [34] Terry J. L. et al 2005 J. Nucl. Mater. 337 322
- [35] Liu S. C. et al 2020 Nucl. Fusion 60 082001
- [36] Liu S. C. et al 2023 Nucl. Fusion 63 042003
- [37] Wang H. Q. et al 2014 Phys. Rev. Lett. 112 185004
- [38] Ye Y. et al 2017 Nucl. Fusion 57 086041